Beam optics study on a High efficiency Two-stage Multi-beam Klystron for the Future Circular Collider

J.C. Cai, U.N. Zaib, I. Syratchev, G. Burt

Abstract— **The innovative high efficiency (HE) Two-stage (TS) Multi-beam Klystron (MBK) technology has recently attracted significant research attention due to its compactness and high efficiency performance. However, there is still a lack of scientific research on the beam optics for such microwave power sources integrated with an post-acceleration (PA) gap. In this paper, a comprehensive optics study based on newly-developed 2D optics code CGUN is conducted for the first time to demonstrate the most critical steps in the optics design process, by adopting the 400MHz TS MBK for the Future Circular Collider (FCC) as an example. Two specific challenges arise in HE TS MBK that do not appear in other tubes, which in this paper are studied and solutions for each is given. Firstly due to the combination of slow electrons, impedance change when transitioning from individual beamtubes into common volumn, and the mild decay of the magnetic field, there are possible reflected electrons at the collector entrance. This requires an increase in the beam voltage to 80 kV, beyond the requirements from considering the output gap alone, as well as tighter control on bouncing electrons. The beam scalloping is also found to be highly sensitive to the position of the PA gap and magnetic field, which later demonstrates that large gap length and magnetic field is required. Final all-in-one particle-in-cell (PIC) simulations of this Klystron equipped with this special optics design demonstrate that the specification of 1.2 MW CW power is attainable with an efficiency of 77.5% and without the presence of reflected electrons at any point in the whole circuit.**

Index Terms—**TS MBK, High efficiency, reflected electrons.**

I. INTRODUCTION

Two stage MBK's utilize a post-acceleration (PA) gap to divide the Klystron circuit into a low voltage part for a short-distance bunching process, and a high voltage part for high-efficiency power extraction [1,2,3]. Study of the beam-wave interaction on a variety of TS MBK configurations shows that it has a prominent application potential for relatively low-frequency (S-band and below) high-power devices, considering its conventional klystron counterpart is much longer and less energy efficient [4,5]. Large particle accelerator complexes, such as CLIC and FCC, in an under-ground tunnel environment prioritize Klystrons with both energy economy and compactness [6]. For instance, a prototype 1.2MW, 400MHz Klystron has been recently proposed and designed at CERN for the FCC project under the stringent requirement for a total length of fewer than 3m and a conversion efficiency close to 80%. As a comparison, Thales commercial TH2089 Klystron with a similar operating frequency and output power level is

5.5m long and 63% efficient [7].

The fundamental TM_{010} mode of a pillbox cavity is primarily selected for the beam-wave interaction to maximize the effective impedance for this MW Klystron [8]. The beam tunnel radius is set as 10.8mm to compromise between having a suffient coupling coefficient and low current density with beam loading. Limited by the transverse dimensions, up to ten beamlets can be utilized to minimize the beam perveance, which is prerequisite for high efficiency performance [9]. The most challenging part is to fix the total beam voltage with a constant beam power of 1.56MW.

It was later found that choosing the proper beam voltage is not only determined by beam-wave interaction analysis, but also constrained by spent beam optics in the RF state, specially by the occurrence of reflected electrons originated at the entrance of the collector rather than output gap, which will be demonstrated in Section II. This unique problem is brought by very slow spent beam electrons after HE power conversion, special mechnical arrangement of TS components to facilitate the assembly and closely located beam tunnels adopted in fundamental cavities. Therefore, appropriate low beamlet perveance has to be utilized to eliminate possible reflected electrons without siginificantly increasing the circuit length. After the voltage of 80kV and beamlet current of 3A is fixed upon such constraints, new optics features in TS MBK brought by PA gap will lead to a new methodology of PA gap design and selection of magnetic field to control the beam scalloping with obtuse sensitivity to precise gap location and magnet accuracy, which will be elaborated in Section III. Newly developed and finished CERN 2D optics code called CGUN is equipped with internal magnetic module supports 2-D B-field mapping and external E-field import functions. This extends its capacity and accuracy to simulate spent beam optics in collector region, providing the capability to simulate every aspect of preliminary optics design from the cathode to the collector. Based on CGUN 2D design comprehensively presented in Section III and IV, the sophiscated optics of multiple hollow beamlets in 3D scenario with/without RF are deomonstrated in Section IV, further validating the whole optics design. Conclusions will be made in Section V.

II. REFLECTED ELECTRONS ISSUES

Practically speaking, a lower voltage means a shorter circuit but lower efficiency [10]. Normally, we pursue the lowest possible beam voltage to simplify engineering aspects of the design (power supply, civil economy, etc). A rough estimation by KlyC shows that a 60kV beam voltage should ensure 80% efficiency [11]. A key aspect in klystron design is the avoidance of reflected electrons which can cause instabilities by providing

Jinchi Cai (jccai@uestc.edu.cn) is with School of Electronic Science and Engineering in UESTC (University of Electronic Science and Technology of China), Chengdu, China. Zaib un Nisa and Igor Syratchev (igor.syratchev@cern.ch) are with BE/RF group at CERN (European Organization for Nuclear Research), 1211, Geneva 23, Switzerland. Graeme Burt (graeme.burt@cockcroft.ac.uk) are with Department of Engineering of Lancaster University, LA1 4YW, Lancaster, United Kingdom;

a feedback loop between cavities. Based on consideration of the output gap alone, a 60 kV beam voltage should allow stable operation without causing reflected electrons in the main RF circuit including the output gap. However, it was found when modelling a preliminary version of this HE TS MBK in CST including simple coaxial collector, that reflected electrons will indeed occur at the interface region between the exit of the individual multi-beam tunnels and the common volume at the collector entrance, where transient efficiency fluctuated around 76% [12]. The occurrence of reflected electrons is due to the sudden potential drop caused by the abrupt structure change, and hence impedance, from the individual beam tunnels to the common collector volume. Such a topology has to be used in this case, rather than implementation of individual collectors, as there is a physical spacing constraint to avoid transverse overlapping in this fundamental MBK. The high total current and low voltage of the beam after high efficiency extraction further worsens the space charge depression around this interface. It should be noted that it is proposed that in this TS MBK no iron plate is used near the collector entrance on the tube body. This is to facilitate the assembly of the magnet/coils from the collector side due to the extra mechanical parts required for the PA gap and the high-voltage insulated input coupler. Therefore, the radial expansion rate and off-axis bending of the beamlets is quite mild near the interface where the magnetic field is still close to saturation. It should also be aware that the interface could not be put too far where magnetic field is decaying low, since heat dissipation by beam scrapping on the tunnel wall could not be cooled down efficiently because of tight spacing.

A numerical study was then performed on spent beam optics illustrated in Fig.1, using a short CST PIC model consting of only the output cavity and the interface to the coaxial collectror region with an ideally bunched emission beam immersed in strong uniform magnetic field [12]. The aim of this study was to determine the lowest acceptable velocity of the spent beam entering the collector with a high efficiency interaction. In this model, the external quality factor is optimized to ensure the RF efficiency is around 80%, then the bunch length of the modulated emission beam is further adjusted to vary the lowest velocity with the interface sealed. The threshold of lowest velocity can be dete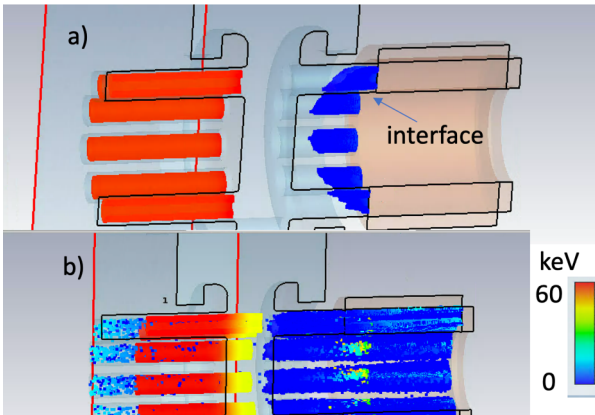rmined when the interface is open by observing the occurrence of reflected electrons. These quick simulations show that the minimum ratio (v_e/c) should be above 0.05 (600eV) to avoid reflected electrons for a 60kV case, while such value for previous design is below 0.03. Following this prediction, KlyC simulations are used to re-design the Klystron with such constraint [12]. By scaling and post-optimization of a 1GHz, 20MW TS MBK design, the maximum scaled efficiency can be evaluated as 73.5% in the disk-code KlyC [1,12]. Due to 3D effects, typically the efficiency in 3D PIC simulations will be 2~3% lower than KlyC results, so a 60kV design is not acceptable [1]. Therfore, a higher beam voltage with a lower beam perveance were then considered in the PIC model mentioned above. Further numerical study demonstrates that when the goal efficiency is set as 80%, the acceptable min(v_e/c) could be improved to 0.04 (400 eV) while avoiding reflected electrons from the interface when using a higher beam voltage of 80 kV. Under this constraint the conversion efficiency can reach up to 80.3% after KlyC optimization, which is consistent with the target efficiency. For comparison, if 70kV is adopted, the simulated efficiency in KlyC will be reduced to 77.7% with the same design process. This quick study based on the iteractive process using both KlyC and short PIC models shows that 80kV is the minimal beam voltage to achieve an HE output (~80%) without the risk of introducing reflected electrons in the collector entrance region, where the velocity spread is shown in Fig. 2. As klystrons operate over a range of powers, it should be noted that bouncing electrons are intentionally avoided in these KlyC simulations to ensure min(v_e/c) will always be above this threshold (0.04) even when the input power is less than the saturatated level, thus making the tube stable in the entire operating power range. Based on these results, 80 kV and 1.95 A are selected as the operating beam voltage and current respectively for this TS MBK.

Reflected electrons in this HE TS MBK are more likely to occur in the interface region between the output cavity and the collector rather than in output gap, which leads to a more complicated collaborative design process presented in this Section. This inherent chanllenge is brought on by the strong mangetic field required by the two-stage mechanical structure, the sudden impedance drop by the multi-beam topology and the ultra-slow electrons in the spent beam induced by the high efficiency conversion. Another source of reflected electrons could come from the collector space itself which will be addressed in Section IV. The secondary electron yield is normally not a major issue for non-depressed collectors and
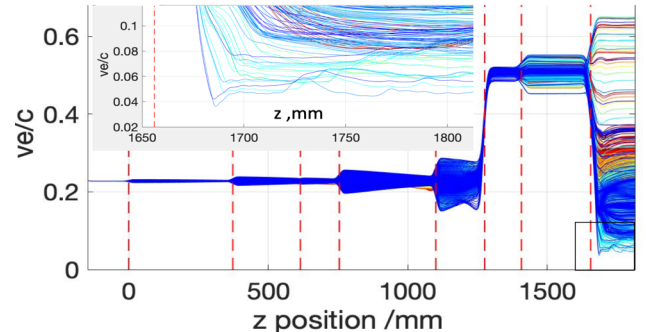

Fig. 1. Output cavity standalone model to consider reflected electrons around collector entrance. a) Interface closed. b) Interface open.

Fig. 2. Velocity spread simulated by KlyC.

could be suppressed by some universal approach such as a material coating [13,14].

III. BEAM OPTICS WITH PA GAP

The voltage for the first and second stage are chosen as 14 kV and 80 kV, respectively, according to the KlyC optimization results, thus the post-acceleration gap should provide a DC voltage of 66 kV. The change in the image charge when the electron bunch traverses the gap will cause the beam to radiate into the PA gap, leading to beam energy loss reducing the efficiency. Previous simulations show that the gap length will barely affect the beam-wave interaction but will have a critical influence on the radiation power emitted from the PA gap which behaves like a radial transmission line, even if a choke structure is utilized to prevent the radiation from escaping the gap [1], as shown in Fig.3a). Compared with previous design in [1], the inner hollow structure is abandoned and replaced by proper setting of the radial position of the choke to detune the traped modes. A 3rd harmonic choke is applied on the outer most layer to further damp the radiation at higher harmonics. The radiation spectrum, as measured by the gap voltage at a large radial position, for a gap length of 30 mm is shown in Fig.3b), demonstrating that an optimized choke structure can effectively suppress the power leakage of the microwaves. The final determination of the gap length is not a straightforward random choice, and several critical aspect such as power radiation, DC breakdown and beam scalloping should be considered. The power of the radiation and its maximum electric field as the function of gap length is shown in Fig.3c). A bunched beam with the modulation depth predicted by KlyC is injected into the structure for this evaluation. To avoid considerable radiation heating outside of the structure and possible positive feedback leading to self-oscillation, 10 W is chosen as a rough limit to leave some margin for bandwidth and assembly errors. 10 kV/mm is set as a hard limit for the DC sparking threshold in vacuum, therefore, a 20~30 mm gap length is taken as compromise between the 2 effects. Normally, a larger gap length provides a reduced transverse electric field generated from both sides of the PA gap which results in a lower confining magnetic field to achieve the same level of beam scalloping after the gap. Therefore, a 30 mm is primarily determined for
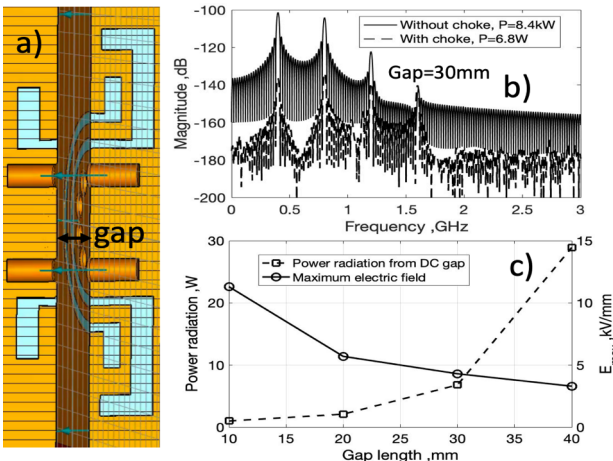
the PA gap length and a 20 mm counterpart will be taken as comparison to verify that a large gap is optimum.

Beam-wave interaction analysis by KlyC shows that the whole circuit length between the input and output cavities could be kept within 1.65 m. A hollow beam with an outer radius of 7.6 mm and an inner radius of 4mm is adopted here for both efficiency and stability enhancement. The CERN 2D optics code CGUN is then intensely used for fast beam optics studies including beam generation, transmission and collection in this special beam-optics system [15]. CGUN has been developed with a classic electrostatic module, magnetostatic module and a beam dynamics module in its package, based on classical mathematical methods deployed by other 2D beam optics codes such as EGUN and DGUN [16,17]. One of the advantages of CGUN is that as the magnetic simulation is internally supported in this package. The 2D magnetic field mapping is either indirectly generated by the axial magnetic profile for paraxial cases or directly imported for the selected region for more general situations [18,19]. Another sustainable advantage is that more specific or user defined features can be added to meet requirements, such as the PA feature and the deployment of external fields to decelerate the beam with energy spread for spent beam diagnosis. The current density of the beamlets in the circuit is 1.5 A/cm^2 which indicates a non-convergent Pierce gun could be used as it is well below the long-life threshold for normal thermionic cathodes. A uniform immersive magnetic field is used in this non-convergent design, so the sub-system before the collector is nearly axially symmetric around each local axis of each of the beamlets ignoreing the negligible beam-beam interference [1,20]. The non-convergent pierce gun with a plane cathode was then designed following classic methods [21], by adopting the proper design of a control electrode to compensate for the radial deflection force imposed by the anode entrance, shown in Fig.4a). An immersive magnetic field is still required to confine the electron trajectories where 0.05T should be sufficient, which is indicated in Fig.4b). The uniformity of the current emission density on the cathode surface is within 15% with a total space-charge limited current of 1.96 A, shown in Fig.4c). It is worth mentioning that such a 2D simulation in CGUN takes about 2 minutes for each case with a mesh number of 1 million and 20 minutes for 20 million on mainstream PC, thus making it a very useful tool for fast optimization. In all these preliminary optics
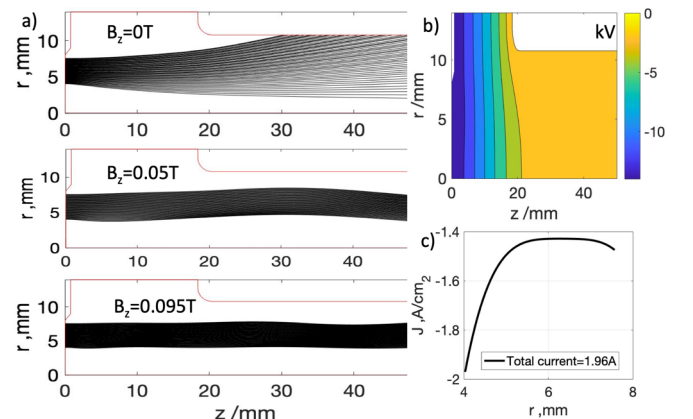
Fig. 3. Post-acceleration gap. a) PA geometry b)Radiation spectrum c)Radiation power and E$_{max}$ as function of gap length.

Fig. 4. Non-convergent electron gun a) beam trajectory in different B$_z$ b) Potential distribution c) Emission current density.

studies, it is assumed that the RF modulation of the beam current will not introduce a significant perturbation to the beam optics before power extraction. Therefore, the PA gap design will mostly be done in the DC scenario, in which electro-static and magneto-static forces dominates the process. Mild RF perturbation effects will be presented in the final Section.

Due to the previously aforementioned PA gap issue, the magnetic field and length of the PA gap will greatly affect the beam optics after the PA gap so extra attention should be paid there. With the implementation of a PA gap, extra static transverse electric fields appear on both sides of the gap trying to compress and expand the beam which imposes heavier beam scalloping after the PA gap even though the beam perveance is reduced after acceleration. This electron behavior requires a strong uniform magnetic field for envelope confinement in the whole circuit especially after the PA gap. For instance, if a typical magnetic field of 0.05 T, which is about 3 times of Brillouin magnetic field, is used, the beam scalloping in the first stage is smooth but becomes unacceptable in the second stage due to this transverse kicking effect, shown in Fig.5. It is noteworthy that the exact location of the gap will considerably affect the envelope rippling in the second stage, which depends on the relative position of the beginning of the gap whith respect to the phase of the envelop ripple from the first stage. Such physical effects can be explained by transerve force counteraction between the magnetic-space charge force and the static electric force from the PA gap. For example, envelope scollaping could be mitigated if the incoming beam at the beginning of the PA gap is expanded radially so that it will balance the transerve kicking force from the PA gap to a certain degree. By slightly adjusting exact position of the DC gap to change the matching status, the best and worst scenarios are demonstrated in Fig.5b) and Fig.5c), respectively. The envelop
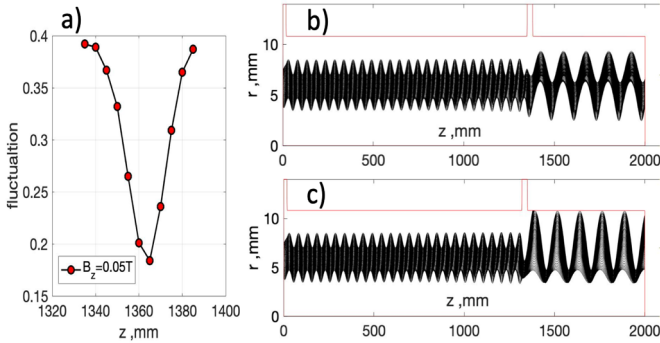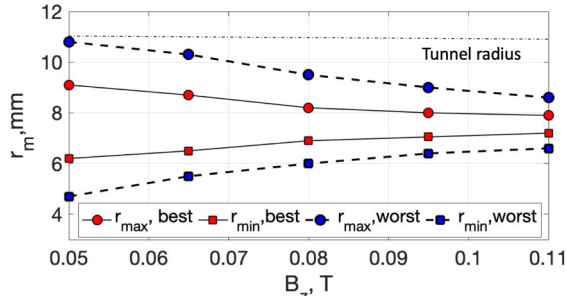
fluctuation $(r_{max}-r_{min})/2/r_{average}$ as a function of the location of the gap center is shown in Fig.5a). This position adjustment is equivalent to a slightly varying magnetic field which also changes the phase of envelop fluctuation at the beginning of PA gap. It is generally known that in the case of electron movement in a magnetic field, that the period of the envelop oscillation is inversely proportional to the magnetic field, thus 1% variation on the magnetic field will correspond to a 25% phase shift in one ripple period, if there are 25 periods ahead of the PA gap. This could result in the envelope flucation being perturbed by up to 50%, taking the case in Fig.5a) as an example [21,22]. Overall such effects are very sensitive to the B-field and the relative gap locations so that it should be taken as an error bar which should always be confined within our acceptable range, to provide flexibility for the mechanical design or magnet design.

2D simulations in CGUN demonstrate that a larger magnetic field should be applied to mitigate the overall envelope scalloping. Since the beam scalloping in the first stage is much smaller compared with that in the second stage, only the information about the second stage is collected in Fig.6. The solid line indicates the maximum and minimal radius of the beam envelope in the best case scenario, while the dashed line shows such properties in the worst case scenario. Bz is finally chosen as about 0.095T to preserve sufficient beam-tunnel clearance, for which the beam trajectories of the best and worst case scenarios are demonstrated in Fig.7a) and Fig.7b), respectively. It should be noticed that the difference between Fig.7a) and b) is fairly small, therefore, in more general situations where some there are some parameter errors, such as the model demonstrated in Section III, the perturbed beam optics will barely affect beam transmission, power extraction or spent beam collection. As verification of the aforementioned statement that beam scalloping would become worse when the gap length is reduced to 20mm, more simulation results are shown in Fig.7c) and Fig.7d), where the magnetic field is fixed as 0.095 T for comparison. This is indeed consistent with our previous speculation.

Fig. 5. Beam envelop in TS MBK with magnetic field of 0.05T for gap length of 30mm. a) best scenario b)worst scenario.

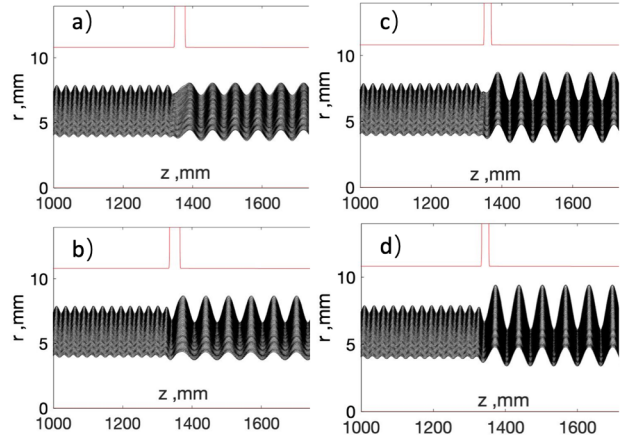Fig. 6. Beam envelop in 2nd stage as function of magnetic field.

Fig. 7. Beam optics with magnetic field of 0.095T. a) b) best/worst scenario for gap length of 30mm c) d) best/worst scenario for gap length of 20mm.

IV. 2D/3D BEAM OPTICS DESIGN

The magnetic system comprises of an iron shield and current coils, which was designed in CGUN and later verified by the
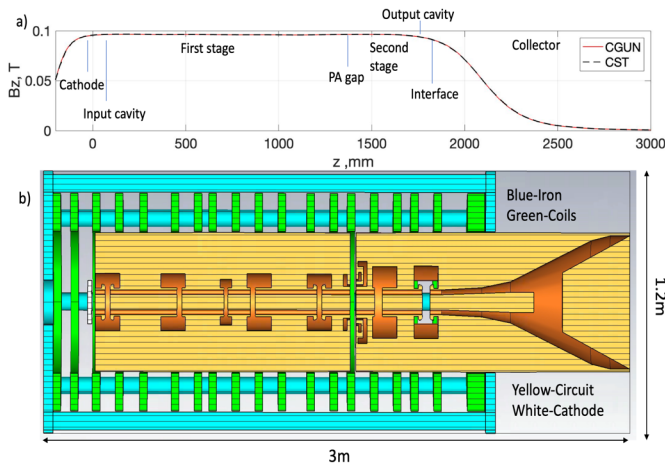
Fig. 8. Magnetic system for TS MBK a) Axial magnetic profile for TS MBK b). Overview of Magnet and Circuit locations.
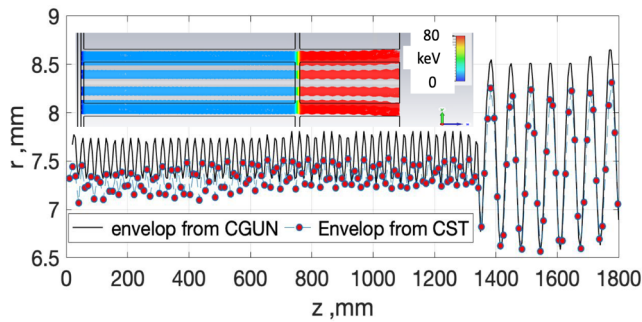

Fig. 9. 98% Beam envelops evolution in CGUN and CST.

Fig. 10. Beam trajectories in collector simulated in CGUN a) with Paraxial assumption. b) with 2D field imported c) imported B_z distribution.

Fig. 11. Power dissipation on collector surface a) RF case. b) DC case.

CST magneto-static solver, shown in Fig.8a). As the axial magnetic field is almost uniform in both the gun and the RF circuit, there is nearly no transverse magnetic field before the entrance of the collector for each beamlet which leads to a radial offset. The relative location of the Klystron circuit and magnet are also schematically shown in Fig.8a) and its 3D models are illustrated in Fig.8b) to have a panoramic view of the whole optics system. The beam envelopes (defined as containing 98% of the whole current) in DC case could be monitored both in the 2D code CGUN and in a 3D code using CST's TRK module, demonstrating good consistency with each other in the uniform magnetic field region before and after PA gap, as illustrated in Fig.9. Multiple hollow beam topology are employed for 3D optics design, proving that beam-beam interference is convincinly negligible. The space-charge limited current for each beamlet is about 1.95 A in CST TRK with variation less than a half percent. The above benchmark effort shows CGUN is a very reliable tool for fast optic simulation, considering 3D multi-beam trajectory simulations to handle similar problems takes at least 10 times longer using convergent mesh settings.

The next step is to design the collector. To facilitate such a design in a 2D situation, large hollow electron beams are modeled to resemble the 3D multi-beam topology, by azimuthally averaging the current density in the emission plate. To realize 2D beam optics simulations for RF scenarios in CGUN, electrons are divided into several groups at one emission point. Then the different groups will experience different deceleration fields in the output gap region to imitate the energy spread in a spent beam, from which information could be obtained from the beam-wave interaction simulations in KlyC. The bulk of the magnet and iron, which is transversely
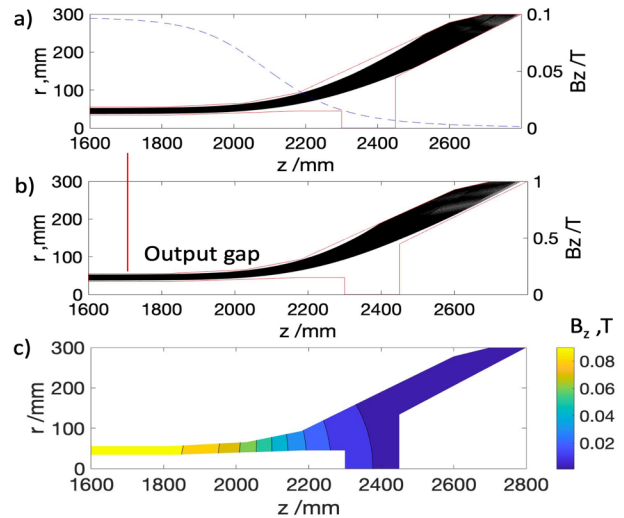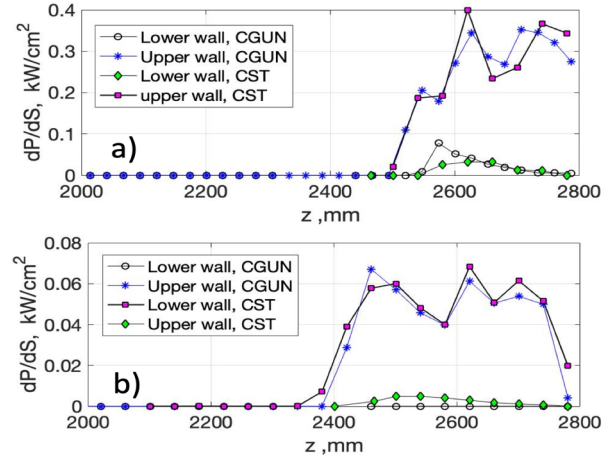
separate but close the to tube illustrated in Fig.8b), shows the mild decay of the magnetic field after the RF circuit which allows the radial expansion and bending of the spent beam inside the collector volume. Based on such a simplified 2D model, a compact collector profile was optimized in CGUN with the goal to ensure the average power dissipation density on the copper wall was less than empirical threshold of 0.2 kW/cm², thus making water cooling possible according to industrial practice. It should be noted that since the electron trajectories in a large hollow beam actually propagate in far off-axis regime, magnetic field mapping in such off-axis area has to be used directly rather than expanding axial magnetic profile by the paraxial symmetry assumption. The discrepancy of such effects is illustrated in Fig.10a) and b), by using the RF case as example. The 2D B_z distribution calculated by CGUN is also plotted for comparison shown in Fig.10c), whereas B_z is constant along radial postion for paraxial approximation if only axial magnetic profile is provided in Fig.10a).

The power dissipation density for the DC and RF cases simulate by CGUN and CST PIC (which will be elaborated later) are demonstrated in Fig.11a) and b), respectively. Consistency between the 2D model in CGUN and 3D CST model proves that both the large hollow beam approximation and energy spread handling techniques are valid methods. This is due to the fact
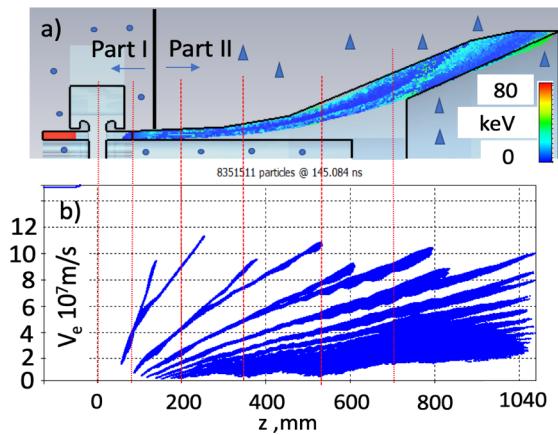
Fig. 12. Phase space diagram of spent beam in collector. a) collector profile with beam. b) phase space diagram.

that the spent multi-beamlets in the collector will mix with each both spaciously and transiently, averaging every modulated paramters evolved from the prior process. In the collector profile design, apart from in the CGUN 2D code for thermal loading control, a model similar to that used in Fig.1 is also used to check for the possibility of reflected electrons after tentative CGUN design is performed for power dissipation control. By attaching the designed collector profile into this short PIC model, illustrated in Fig.12a) and real magnetic field, the analysis techniques aforementioned in Section II is adopted. More specifically, the efficiency is set up as 80% with $\min(v_e/c)=0.042$ in which model the interface is placed outside the simulation volume to get closer to the situation predicted by the KlyC simulations shown in Fig.2. The observation of the prescence of reflected electrons will provide a check if the collector profile near the interface is properly designed. This iterative process could guarantee both reasonable thermal loading and suppression of reflected eletrons. There are some design aspects worth mention 1) The interface itself will not introduce reflected eletrons anymore due to the selection of the beam parameters in Section II. 2) The outer surface of the collector is designed to be close to the beam edge to mitigate retarding space-charge fields generated by the slow spent beam. 3) The inner conducter has to be placed near the entrance of the collector and extended for some distance to further reduce the potential barrier until beam is fully expanded radially and starts to intercept, as the space charge density will significantly reduce then. This is important as reflected electrons in collector will occur when the inner conductor is removed or too short. The gap length here is a compromise between minimizing the weight of inner conductor and the mitigation of the space charge potential drop in this region.The phase-space diagram for the final adopted collector design is plot in Fig. 12b) ,showing no reflected electrons will occur in whole collector range whereas each local bump of the slowest velocity evenlop corresponds to the sudden potential drop caused by the geometry evolution. The gap between the inner conductors in the collector and cavity regions is also to ensure convenient assembly of the collector in 2 parts, where the inner part is attached to the main body on the left and other parts of the collector could be inserted from the right and brazed, which is also demonstrated in Fig.12a), distinguished by circular dots and triangle dots.

This collector design was then verified by all-in-one CST PIC simulations. The emission beam set up near the entrance of the anode is directly imported from the CST TRK module and then transmitted through the RF circuit during which the velocity modulation is gradually transformed into a charge density modulation, before its power is extracted in the output gap. Every structure detail such as the multi-beam cavity geometry, the choke in post-acceleration gap and the optimized collector shape are included in this 3D model, where the 3D magnetic field map is imported from the CST magnetostatic solver directly. The number of mesh elements and the peak number of particles in this simulation are around 50 million and 100 millon, respectively. It takes about 4 days to finish a 1000 ns pulse simulation of this TS MBK on a CERN workstation equipped with up-to-date Duo 32 GB Quadro GV100 GPUs, a 32 core 4.0 GHz CPU and 383 GB internal memory. The simulation results show that the azimuthally averaged power dissipation in CST agrees quite well with the CGUN results in both the DC and RF scenarios, shown in Fig.13a) and Fig.13b), respectively. Further post-processing diagnosis shows that the peak power dissipation is about 3~4 times the average value in the DC case and about 2~3 times the average value in the RF case. Therefore, such a Klystron could operate in CW mode in the RF scenario with marginal overhead to avoid overheating hot spot due to possible misalignment or parameter errors. More 3D plots of the beam optics in different perspectives are shown in Fig.13a), in which the multi-hollow-beam structure can be clearly observed in the DC mode. The trajectory overview as a result of the beam-wave interaction in the RF mode is shown in
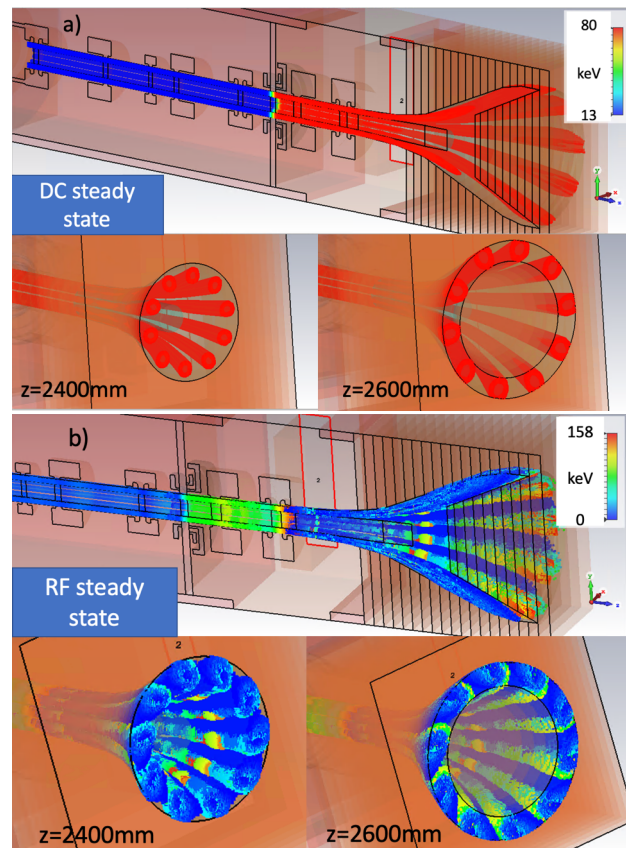

Fig. 13. 3D plot of beam optics in all-in-one simulation a) DC scenario. b) RF scenario.
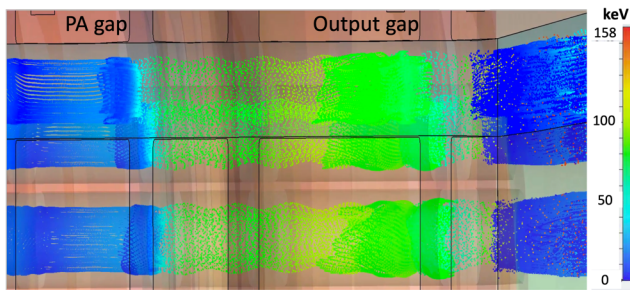
Fig. 14. Beam optics in PA and output gap in RF scenario.

Fig.13b) and demonstrates that no reflected electrons are spotted until steady-state. The 3D Beam optics in the PA gap and the output gap in the RF state is illustrated in Fig.14, which indicates slightly worse beam scalloping due to RF bunching effects but still provides sufficient beam-tunnel clearance for later transmission and power exchange. As strong magnetic fields have been used, radial expansion due to power exchange is also highly mitigated in the output gap, also shown in Fig.14. It can clearly be observed in Fig.13a) that there is no evident diocotron instabilities during the whole transmission section for each individual hollow beamlet due to the large thickness of the hollow beamlet, relatively high magnetic field and compact TS arrangement [23]. The saturated operating point without reflected electrons demonstrates that such a Klystron could stably deliver output power up to 1.2 MW at 400 MHz with an efficiency up to 77.5%. The slowest velocity of electrons in the full 3D model is close to the value predicted in Fig.14, validating our design process while showing that the RF saturation state is really close to the optimum performance for this TS MBK with the guarantee of stability. This practice validates the whole specific beam optics design effort for this innovative HE TS MBK, which can be taken as reference in case similar work has to be conducted in the future.

V. Conclusions

The comprehensive beam optics study has been reported for the first time for the innovative HE TS MBK design for FCC. Special and critical considerations regarding the methodology on suppression of reflected electrons, determination of the post-acceleration gap and the magnetic field strength have been firstly studied and discussed. The newly-developed CERN code CGUN is proven to be a reliable 2D optics analysis tool for fast and accurate simulations of such multi-stage devices from cathode to collector, with multiple useful features implemented. All-in-one PIC simulations validate the whole optics design both in DC and RF scenarios, demonstrating that a 400 MHz 10 beamlets TS MBK could stably deliver an output power of over 1.2 MW with efficiency of 77.5% (80% predicted in KlyC) where total beam voltage and current is 80kV and 19.5A, respectively. The whole optics system length of 3 meters with diameter of 1.2m indicates the whole Klystron package could be controlled within this compact dimension regarding the relatively low frequency regime, provided other mechanical components are properly designed and implemented.

References

[1] J.C. Cai and I. Syratchev, "Modeling and Technical Design Study of Two-Stage Multibeam Klystron for CLIC", *IEEE Transactions on Electron Devices*, vol. 67, no. 8, pp. 3362-3368, Jun. 2020, doi: 10.1109/TED.2020.3000191.

[2] V.E. Teryaev, S.V. Shchelkunov and J.L. Hirshfield. "Concept and simulations of 800MHz Two-Stage MBK for FCC," *IEEE Transactions on Electron Devices*, vol. 68, no. 3, pp. 1271-1275, Jan. 2021, doi: 10.1109/TED.2021.3052722.

[3] V.E. Teryaev, S.V. Shchelkunov and J.L. Hirshfield. "Innovative Two-Stage Multibeam Klystron: Concept and Modeling," *IEEE Transactions on Electron Devices*, vol. 67, no. 7, pp. 2896-2899, May. 2020, doi: 10.1109/TED.2020.2991681.

[4] R.K. Parker, R.H. Abrams, B.G. Danly, B. Levush "Vacuum electronics", *IEEE Trans. On Microwave Theory and Techniques*, vol.50 no.3, pp.835-845, March 2002, doi: 10.1109/22.989967.

[5] D.K. Abe, D.E. Pershing, K.T. Nguyen, F.N. Wood, R.E. Myers, E.L. Eisen, M. Cusick, and B. Levush. "Demonstration of an S-band, 600-kW fundamental-mode multiple-beam Klystrons," *IEEE Electron Device Letters*, vol. 26, no. 8, pp. 590-592, Aug. 2005, doi: 10.1109/LED.2005.852540.

[6] P. Lebrun, 'Energy consumption and savings potential of CLIC', 55th ICFA Advanced Beam Dynamics Workshop on High Luminosity Circular e+e- Colliders – Higgs Factory Beijing, 9-12 October 2014.

[7] M.K. Badapanda, A. Tripathi, R. Upadhyay and P.R. Hannurkar,, "Development of 352.2 MHz high power RF test setup", in *IEEE International Vacuum Electronics Conference*, IVEC 2011, Banglore, India, Feb. 2011, doi: 10.1109/IVEC.2011.5747087.

[8] M.R. Boyd, R.A. Dehn, J.S. Hickey, T.G. Mihran, "The multiple-beam klystron",in *IRE* Transactions on Electron Devices, vol. 9, Issue: 3, pp. 247 – 252, May 1962, doi: 10.1109/T-ED.1962.14979.

[9] Z.N. Liu, H. Zha ,J.R. Shi and H.B. Chen. "Study on the efficiency of Klystrons", *IEEE Transactions on Plasma Science,* Vol. 48, no. 6, pp. 2089-2096, Apr. 2020, doi:10.1109/TPS.2020.2988451.

[10] J.C. Cai, I. Syratchev and Z.N. Liu. "Scaling Procedures and Post-optimization for the Design of High-Efficiency Klystrons", *IEEE Transactions on Electron Devices,* Vol. 66, no. 2, pp. 1075-1081, Feb. 2019, doi:10.1109/TED.2018.2887348.

[11] J.C. Cai, I. Syratchev, "KlyC: 1.5D Large Signal Simulation Code for Klystrons", in *IEEE Trans. on Plasma Science*, vol.47, no.4, pp.1734-1741, April 2019, doi: 10.1109/TPS.2019.2904125.

[12] CST 2020. Available at: https://www.cst.com/products.

[13] W. Neugebauer and T.G. Mihran, 'A Ten-Stage Electrostatic Depressed Collector for improving Klystron efficiency', in *IEEE Electron device letters*, vol.19, no.1, pp.111-121, January 1972. doi:10.1109/TED.1972.17379.

[14] A.N. Sharapa and A.V. Shemyakin, 'Secondary electron flow from axially symmetric collector without magnetic field', in *Nuclear Instrumentation and Methods in Physicis Research A*, vol.396, no.2, pp.110-114, September 1997. doi:10.1016/S0168-9002(97)00650-5.

[15] J.C. Cai, I. Syratchev and G. Burt. "Design Study of a High-Power Ka-band High-Order-Mode Multibeam Klystron", *IEEE Transactions on Electron Devices,* Vol. 67, no. 12, pp. 5736-5742, Dec. 2020, doi:10.1109/TED.2020.3028348.

[16] W.B. Hermannsfeldt, "EGUN an electron optics and gun design program", SLAC Nat. Accel. Lab., Menlo Park, CA, USA, Tech. Rep. SLAC-331, Oct. 1988. doi:10.2172/ 6711732.

[17] A. Larionov, K. Ouglekov, "DGUN-code for simulation of intensive axial-asymmetric electron beams", 6th International Computational Accelerator Physics Conference, TU Darmstadt, German, 2000, p.172.

[18] Ken Hayami. High Precision Numerical Integration Methods for 3D Boundary Element Analysis. *IEEE Trans. Magn.* 1990, 26(2): 603. doi:10.1109/ 20.106389.

[19] Li Quanfeng, Numerical Calculations of Electromagnetic Fields and Design of Electromagnets, Qinghua University Press, 2002.

[20] R. Zhang and Y. Wang, 'Six-Beam Gun Design for a high-power multiple-Beam Klystron', in *IEEE Electron device letters*, vol.38, no.6, pp.1337-1344, June 2010. doi:10.1109/TED.2013.2264357.

[21] J.R. Pierce, Theory and design of electron beams. Toronto: D. Van Nostrand Co., Inc., 1954.

[22] J. T. Mendel, 'Magnetic focusing of electron beams', in *Proceedings of IRE*, vol.43, no.1, pp.327-331, 1955. doi:10.1109/TED.1955.278139.

[23] M. Read, R. Jackson, P. Ferguson, G. Nusinovich and R.L. Ives, 'Design of a 10MW, L-band Annular Beam Klystron', in *IEEE Electron device letters*, vol.61, no.6, pp.1836-1841, June 2014. doi:10.1109/TED.2014.2299519.